Supporting Information for

Spin-Hall Topological Hall Effect in Highly Tunable Pt/Ferrimagnetic-Insulator Bilayers

Adam S. Ahmed[1, ‡], Aidan J. Lee[1, ‡], Nuria Bagués[2], Brendan A. McCullian[1], Ahmed M. A. Thabt[1], Avery Perrine[2], Po-Kuan Wu[1], James R. Rowland[1] Mohit Randeria[1], P. Chris Hammel[1], David W. McComb[2,3], and Fengyuan Yang[1,]*

[1]Department of Physics, The Ohio State University, Columbus, Ohio 43210, USA

[2]Center for Electron Microscopy and Analysis, The Ohio State University, Columbus, Ohio 43210, USA

[3]Department of Materials Science and Engineering, The Ohio State University, Columbus, Ohio 43210, USA

[‡]Equal Contributions

Section 1. Scanning Transmission Electron Microscopy Imaging

The top left panel of Fig. S1 shows a lower magnification cross-sectional image of a Pt(5 nm)/TmIG(5 nm)/sGGG(111) sample along the $[1\bar{1}0]$ direction. Because of the similar atomic numbers (Z) between TmIG and GGG (Z_{Tm} = 69 vs. Z_{Gd} = 64 and Z_{Fe} = 26 vs. Z_{Ga} = 31), they are rather difficult to distinguish in the STEM images because of their comparable brightness. It is slightly easier to see the TmIG/sGGG interface at low magnifications. The bottom left and bottom right panel show further magnified images from the regions highlighted in the red and blue boxes,

respectively. A model of the atomic columns in the (111)-oriented TmIG garnet lattice along the [$1\bar{1}0$] direction is included in the top right panel to illustrate the consistency between the expected atomic arrangement and the observed STEM images of our TmIG films.

Nonlinear drift distortion in the high angle annular dark field (HAADF) scanning transmission electron microscopy image of the plan-view specimen was corrected using Nonlinear Drift Correction from Scanning Probe Microscopy (SPM) Orthogonal Image Pairs MATLAB collection of scripts (Copyright © 2016, Colin Ophus).[1]

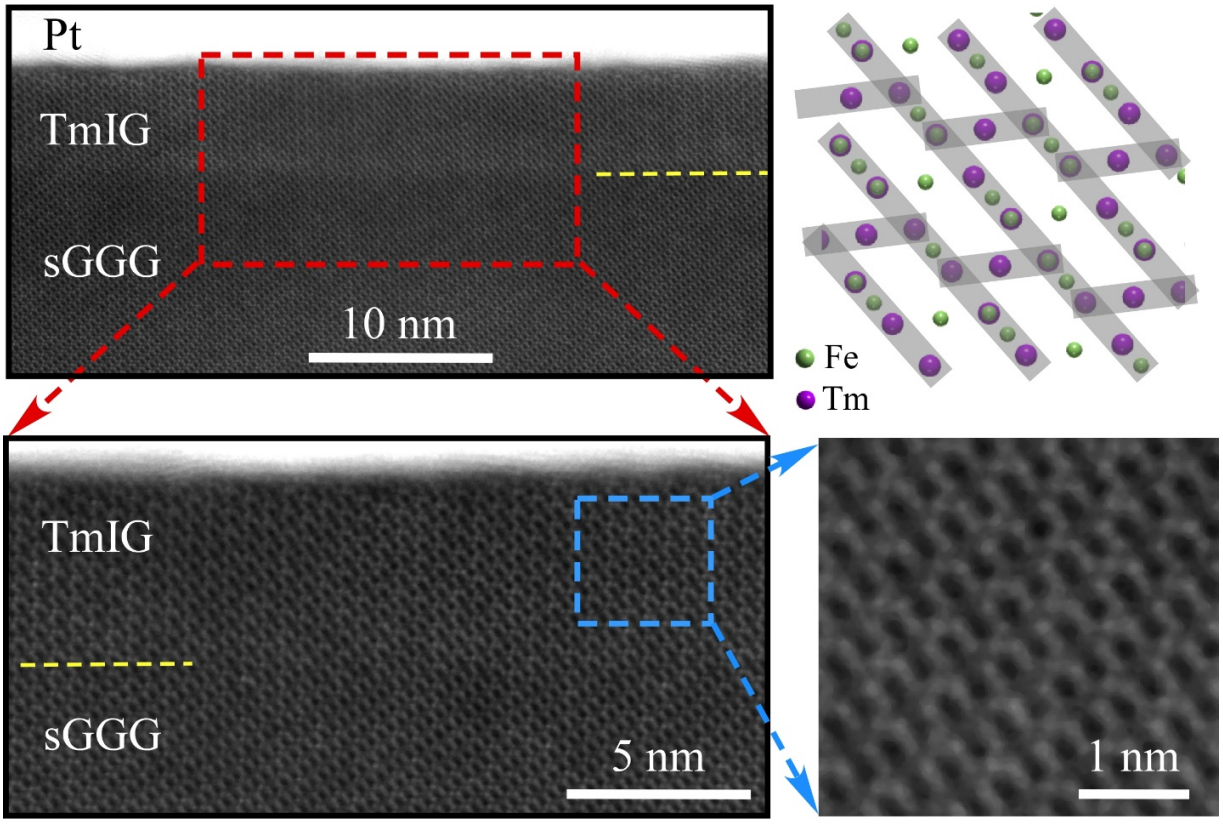

Figure S1. Cross-sectional scanning transmission electron microscopy imaging. Top left, bottom left, and bottom right panels show cross-sectional images of a Pt(5 nm)/TmIG(5 nm)/sGGG(111) sample at various magnifications along the [$1\bar{1}0$] direction. The red and blue boxes indicate the region that was magnified in the adjacent panel. Top right panel is the projection of the (111)-oriented TmIG garnet lattice along the [$1\bar{1}0$] direction, where the chains of atomic columns highlighted by the semi-transparent gray belts match the STEM images.

Section 2. Angular Dependent Ferromagnetic Resonance

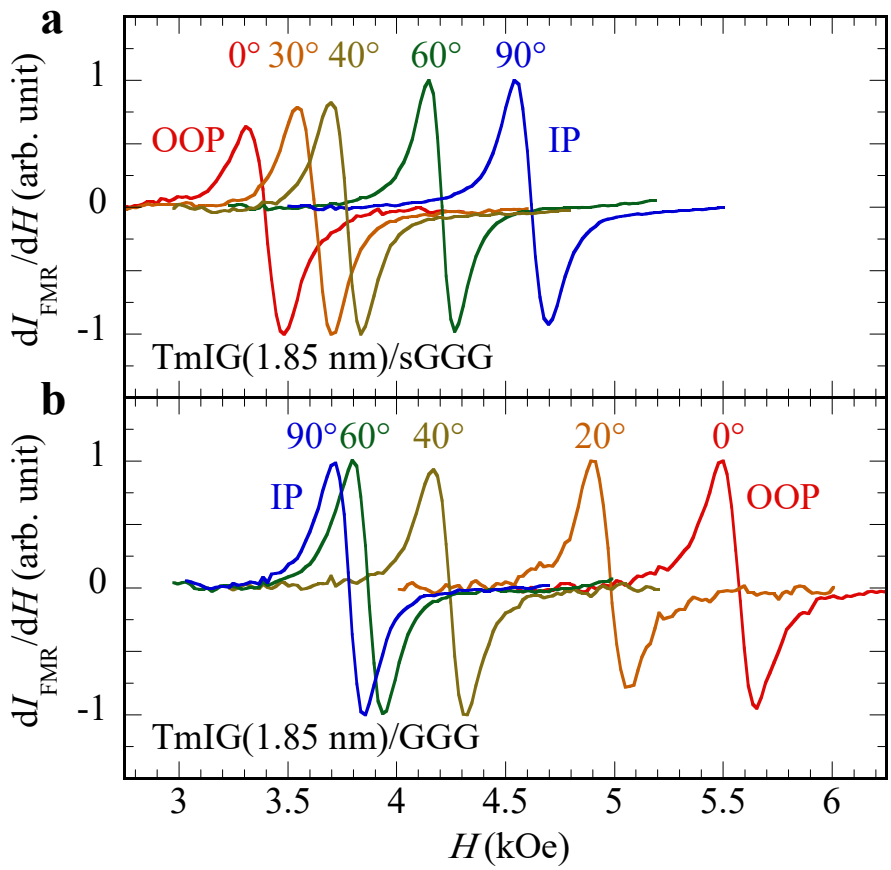

Figure S2. Angular dependent ferromagnetic resonance. a, FMR derivative spectra taken at various polar angles for TmIG(1.85 nm)/sGGG and **b**, TmIG(1.85 nm)/GGG.

Angular dependent ferromagnetic resonance (FMR) spectroscopy was conducted in a Bruker electron paramagnetic resonance (EPR) cavity with a microwave frequency of 9.62 GHz. FMR was utilized to verify that TmIG films grown on sGGG or GGG have perpendicular magnetic anisotropy (PMA) or in-plane anisotropy, respectively, as well as to confirm that TmIG is still ferrimagnetic for very thin films. As an example, Fig. S2a shows the FMR derivative spectra at various polar angles for TmIG(1.85 nm)/sGGG, which has a minimum resonance field at 0° when the field is out-of-plane (OOP) of the film and a maximum at 90° when the field is applied in-plane (IP). This angular dependence of the resonance field indicates that the TmIG grown on sGGG

maintains PMA at room temperature for very thin films.[2] The FMR derivative spectra at various angles is also shown for TmIG(1.85 nm)/GGG in Fig. S2b. The resonance field as a function of angle is shown in Fig. 2d of the main text for the 1.85 nm TmIG films on sGGG and GGG, which exhibit opposite angular dependence, indicating that the TmIG/sGGG has out-of-plane anisotropy while the TmIG/GGG has in-plane anisotropy.[2]

Section 3. Magnetotransport measurements

Pt(3 nm)/TmIG(t) samples on GGG and sGGG were patterned into Hall bars with a 400 μm × 100 μm current channel. A schematic of the Hall bar is shown in Fig. S3, which illustrates the relevant pattern dimensions as well as the locations where longitudinal voltage (V_{xx}) and Hall voltage (V_{xy}) were measured, which were then converted into longitudinal resistivity (ρ_{xx}) and Hall resistivity (ρ_{xy}). Additional Hall resistivity versus magnetic field curves are shown in Fig. S4 for Pt(3 nm)/TmIG(2 nm)/sGGG at a wide range of temperatures where a peak in ρ_{xy} is present at 300 K and persists until 385 K.

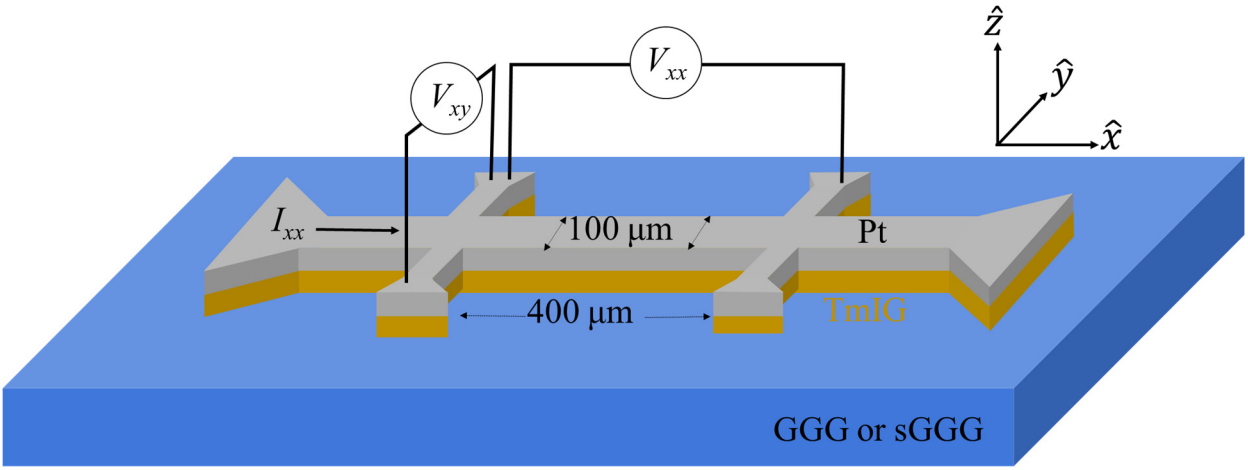

Figure S3. Hall bar pattern. Schematic of the Hall bar pattern created with all of the Pt(3 nm)/TmIG(t)/GGG or sGGG.

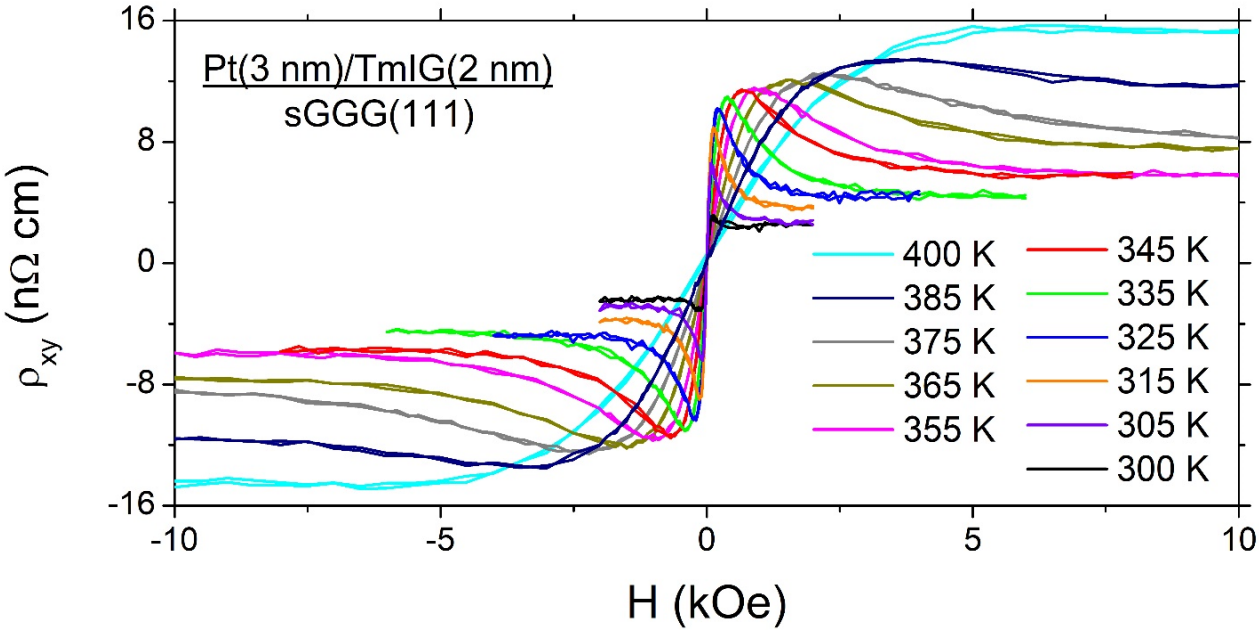

Figure S4. Topological Hall effect in a Pt(3 nm)/TmIG(2 nm)/sGGG(111) bilayer. Hall resistivity versus magnetic field at various temperatures. The peak in ρ_{xy} appears at 300 K and vanishes at $T \geq 400$ K.

All of the transport data shown in the main text was measured using an applied current of 300 μA that resulted in a current density of 1×10^9 Am^{-2}. Various applied currents were also tested to investigate if the current density had any effect on the Hall signal. Figure S5 shows ρ_{xy} as a function of the applied field of Pt(3 nm)/TmIG(1.85 nm)/sGGG(111) at room temperature using various applied current ranging from 25 μA (8.3×10^7 Am^{-2}) to 1000 μA (3.3×10^9 Am^{-2}). All of the data taken with various applied currents lie on top of each other illustrating that there is no current dependence within the current range tested. The lack of current dependence demonstrates that 1) heating effects are negligible, 2) in the current regime explored, the spin torques are not enough to disturb the underlying spin texture, and 3) the transport signal is in the linear transport regime.

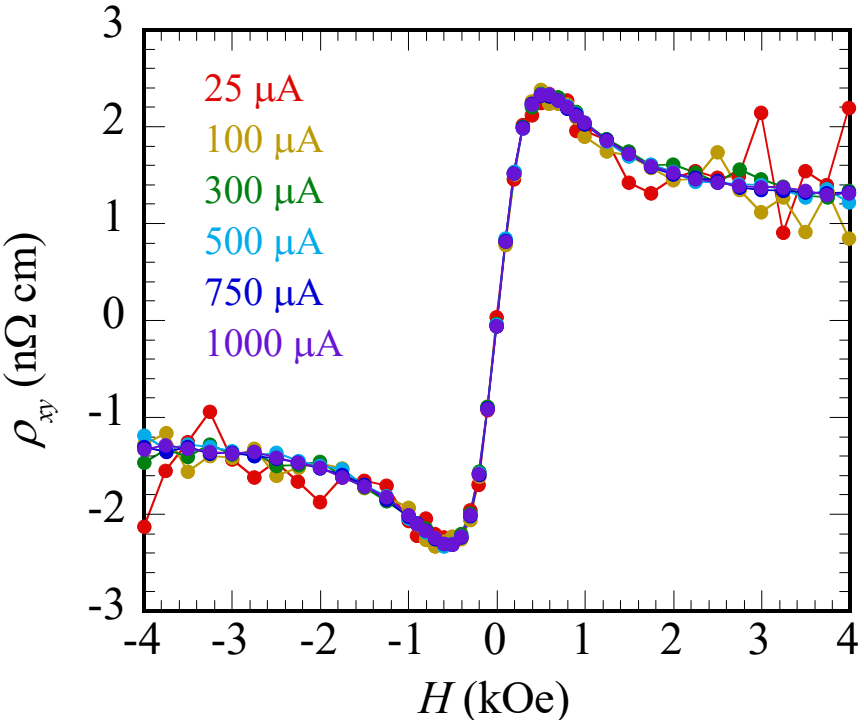

Figure S5. Hall resistivity at using various source currents. Room temperature Hall resistivity loops of Pt(3 nm)/TmIG(1.85 nm)/sGGG(111) with various applied current from 25 to 1000 μA.

We conclude this section commenting on the nature of the spin Hall Topological Hall (SH-TH) effect observed in Pt/TmIG bilayers. Like the spin Hall anomalous Hall (SH-AH) effect, the SH-TH effect is only sensitive to magnetic spin textures at the Pt/TmIG interface and not to the bulk magnetism. However, since skyrmions and topological domains extend through thin films of a few nm thicknesses with $\hat{z}$ symmetry (where $\hat{z}$ is the growth direction), the SH-TH response of the surface topological spin texture should be representative of the bulk.

Section 4. Control experiment to check for the existence of magnetic proximity effect in Pt

To investigate the origin of the topological Hall signal, we performed angular dependent magnetoresistance (ADMR) measurements. If the Pt layer was magnetic by proximity, the magnetic textures that form in TmIG could be imprinted upon the conducting Pt and then a finite

topological Hall voltage would be generated. For heavy metals on ferromagnets, there are three main contributions to the ADMR scans in longitudinal resistivity:[3]

$$\rho_{xx} = \rho_0 + \Delta\rho_{\mathrm{AMR}}\boldsymbol{M}^{\mathbf{2}}_{\mathbf{Pt},x} + \Delta\rho_{\mathrm{SMR}}\boldsymbol{M}^{\mathbf{2}}_{\mathbf{TmIG},y} + \Delta\rho_{\mathrm{OMR}}\boldsymbol{H}^{\mathbf{2}}_{\mathbf{ext},z} \quad \text{(S1)}$$

where ρ_{xx} is the longitudinal resistivity, ρ_0 is the background resistance of the Pt layer, $\Delta\rho_{\mathrm{AMR}}$ is the change in resistance from anisotropic magnetoresistance (AMR), $\Delta\rho_{\mathrm{SMR}}$ is the change in resistance from spin Hall magnetoresistance (SMR), $\Delta\rho_{\mathrm{OMR}}$ is the change in resistance from ordinary magnetoresistance (OMR), $\boldsymbol{M}_{\mathbf{Pt},x}$ is the *x*-component of the Pt magnetization, $\boldsymbol{M}_{\mathbf{TmIG},y}$ is the *y*-component of the TmIG magnetization, and $\boldsymbol{H}_{\mathbf{ext},z}$ is the *z*-component of the external magnetic field. By performing an ADMR scan in the *x*-*z* plane (see Fig. S3), we eliminate the effects of SMR, and the ADMR measurements are only sensitive to AMR and OMR.

During the ADMR scan, the applied field is large enough such that the TmIG magnetization is saturated and $\boldsymbol{M}_{\mathbf{TmIG}} \,||\, \boldsymbol{H}_{\mathbf{ext}}$ at all angles. As can be seen from Eq. (S1), OMR is maximized when $\boldsymbol{H}_{\mathbf{ext}}$ points in the OOP direction. Conversely, AMR is maximized when $\boldsymbol{H}_{\mathbf{ext}}$ points in the IP direction. Thus, AMR and OMR have distinct signatures from one another.

We performed ADMR scans in the *x*-*z* plane at 300 K for a Pt(3 nm)/TmIG(1.85 nm)/sGGG(111) sample which exhibits a prominent topological Hall signal (see main text). This control measurement is to check if a magnetic proximity effect and topological Hall effect are coincident with one another. We define the relative change in the longitudinal resistivity as

$$\Delta\rho_{xx} = \frac{\rho_{xx}(\theta) - \rho_{xx}(0°)}{\rho_{xx}(0°)} \quad \text{(S2)}$$

Figure S6 shows the *x*-*z* ADMR scans for applied magnetic fields of 2 and 14 T (note: the saturation field for this sample is approximately 0.4 T). Here, 0° represents the OOP direction (*z*), and 90° represents the IP direction (*x*). For a 2 T field, there is essentially no angular dependence. However, when the external field is increased to 14 T, only OMR is present as indicated by a

minimum at θ = 90° and 270° with a -sin^{2}θ dependence. There is no detectable AMR which should follow a +sin^{2}θ, i.e., $\Delta\rho_{xx} > 0$; thus, we conclude that the Pt layer is not magnetic and the observed topological Hall signal cannot be from the proximity effect in the Pt layer.

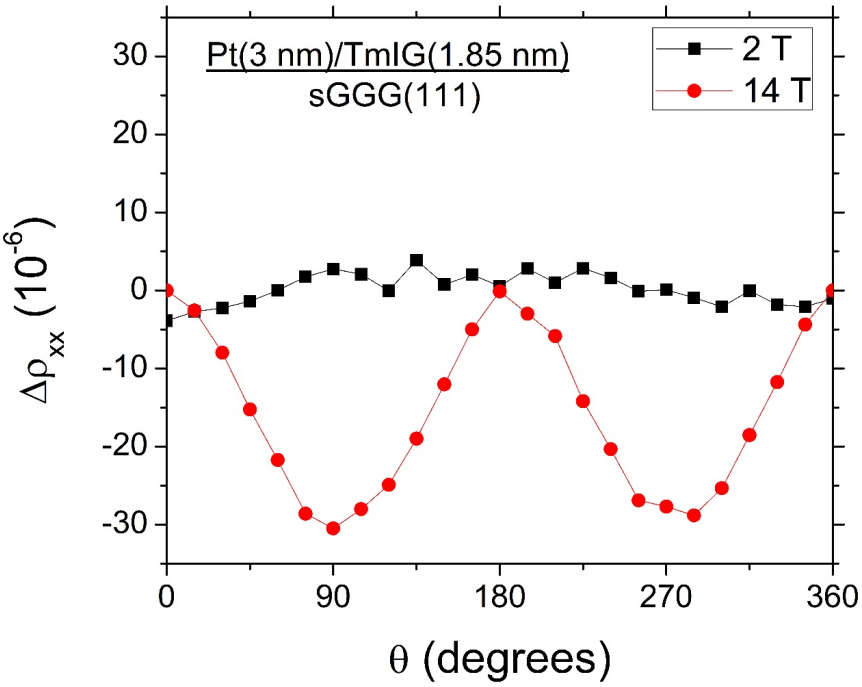

Figure S6. Angular dependent magnetoresistance. Longitudinal resistivity for a Pt(3 nm)/TmIG(1.85 nm)/sGGG(111) sample. At 2 T, there is no detectable AMR or OMR, while only OMR is observed at 14 T.

As a final point, proximity effect usually decreases in magnitude and vanishes at high temperatures.[4] In fact, it is rare that proximity is reported at room temperature. As we still observe a strong topological Hall signal in our Pt(3 nm)/TmIG(3 nm)/sGGG(111) sample at 465 K, this further supports our findings that proximity cannot explain the detected topological Hall signal in Pt/TmIG bilayers.

Section 5. Possible origin of interfacial DMI

In this section, we discuss the possible origin of interfacial DMI at the heavy-metal/ferrimagnetic-insulator interface. The field of interfacial magnetism and skyrmion formation

has primarily focused on metallic ferromagnets like Co and Fe. Furthermore, these experimental and theoretical investigations have focused on metallic heavy metals interfaced with metallic ferromagnets, e.g., Pt/Co or Fe/Ir, where the 3-site RKKY-like interaction is responsible for stabilizing interfacial DMI. More recently, with regards to stabilizing skyrmions, the metallic ferromagnet/insulator interface (e.g. Co/MgO) has attracted interest due to the sizeable DMI that can be stabilized. Such an interface would not support a 3-site hopping interaction where the likelihood of hopping across the metal/insulator interface is significantly reduced. Another mechanism has been proposed to stabilize interfacial DMI at the FM-metal/insulator interface based on the interfacial Rashba effect.[5-8] For example, there are large interfacial electric fields from band bending at metal-insulator interfaces which influence orbital distortions at the interface[9] and change the interfacial DMI.

As the sub-field of skyrmions in heavy-metal/FM-insulator bilayers is at the very early stage, the literature regarding interfacial DMI in heavy metal/FM-insulator systems is quite rare. However, like the FM-metal/insulator interface, large band bending effects would still be present. A theoretical report by Banerjee et al.[10] shows that chiral spin textures, including skyrmions, are stabilized by interfacial Rashba spin-orbit coupling, which gives rise to interfacial DMI, in both Mott insulators and metals. Therefore, we believe that the DMI comes from interfacial Rashba spin-orbit coupling at the Pt/TmIG interface.

Supplemental References:

1. Ophus, C.; Ciston, J.; Nelson, C. T. Correcting nonlinear drift distortion of scanning probe and scanning transmission electron microscopies from image pairs with orthogonal scan directions. *Ultramicroscopy* **2016**, 162, 1-9.
2. Tang, C.; Sellappan, P.; Liu, Y. W.; Xu, Y. D.; Garay, J. E.; Shi, J. Anomalous Hall hysteresis in $Tm_3Fe_5O_{12}$/Pt with strain-induced perpendicular magnetic anisotropy. *Phys. Rev. B* **2016**, 94, 140403.

3. Amamou, W.; Pinchuk, I. V.; Trout, A. H.; Williams, R. E. A.; Antolin, N.; Goad, A.; O'Hara, D. J.; Ahmed, A. S.; Windl, W.; McComb, D. W.; Kawakami, R. K. Magnetic proximity effect in Pt/$CoFe_2O_4$ bilayers. *Phys. Rev. Mater.* **2018**, 2, 011401.
4. Lin, T.; Tang, C.; Alyahayaei, H. M.; Shi, J. Experimental Investigation of the Nature of the Magnetoresistance Effects in Pd-YIG Hybrid Structures. *Phys. Rev. Lett.* **2014**, 113, 037203.
5. Kundu, A.; Zhang, S. Dzyaloshinskii-Moriya interaction mediated by spin-polarized band with Rashba spin-orbit coupling. *Phys. Rev. B* **2015**, 92, 094434.
6. Imamura, H.; Bruno, P.; Utsumi, Y. Twisted exchange interaction between localized spins embedded in a one- or two-dimensional electron gas with Rashba spin-orbit coupling. *Phys. Rev. B* **2004**, 69, 121303.
7. Kim, K.-W.; Lee, H.-W.; Lee, K.-J.; Stiles, M. D. Chirality from Interfacial Spin-Orbit Coupling Effects in Magnetic Bilayers. *Phys. Rev. Lett.* **2013**, 111, 216601.
8. Yang, H. X.; Boulle, O.; Cros, V.; Fert, A.; Chshiev, M. Controlling Dzyaloshinskii-Moriya Interaction via Chirality Dependent Atomic-Layer Stacking, Insulator Capping and Electric Field. *Sci. Rep.* **2018**, 8, 12356.
9. Kim, S.; Ueda, K.; Go, G.; Jang, P.-H.; Lee, K.-J.; Belabbes, A.; Manchon, A.; Suzuki, M.; Kotani, Y.; Nakamura, T.; Nakamura, K.; Koyama, T.; Chiba, D.; Yamada, K. T.; Kim, D.-H.; Moriyama, T.; Kim, K.-J.; Ono, T. Correlation of the Dzyaloshinskii–Moriya interaction with Heisenberg exchange and orbital asphericity. *Nat. Commun.* **2018**, 9, 1648.
10. Banerjee, S.; Rowland, J.; Erten, O.; Randeria, M. Enhanced Stability of Skyrmions in Two-Dimensional Chiral Magnets with Rashba Spin-Orbit Coupling. *Phys. Rev. X* **2014**, 4, 031045.